Noncatalytic regulation of 18*S* rRNA methyltransferase DIMT1 in acute myeloid leukemia

Yulia Gonskikh,[1,6] Julian Stoute,[1,2,6] Hui Shen,[1,6] Krista Budinich,[3,4,5] Bianca Pingul,[1,2] Kollin Schultz,[1,2] Heidi Elashal,[1,2] Ronen Marmorstein,[1,2] Junwei Shi,[3,4,5] and Kathy Fange Liu[1,2]

[1]Department of Biochemistry and Biophysics, Perelman School of Medicine, University of Pennsylvania, Philadelphia, Pennsylvania 19104, USA; [2]Graduate Group in Biochemistry and Molecular Biophysics, Perelman School of Medicine, University of Pennsylvania, Philadelphia, Pennsylvania 19104, USA; [3]Department of Cancer Biology, Perelman School of Medicine, University of Pennsylvania, Philadelphia, Pennsylvania 19104, USA; [4]Epigenetics Institute, Perelman School of Medicine, University of Pennsylvania, Philadelphia, Pennsylvania 19104, USA; [5]Abramson Family Cancer Research Institute, Perelman School of Medicine, University of Pennsylvania, Philadelphia, Pennsylvania 19104, USA

Several rRNA-modifying enzymes install rRNA modifications while participating in ribosome assembly. Here, we show that 18*S* rRNA methyltransferase DIMT1 is essential for acute myeloid leukemia (AML) proliferation through a noncatalytic function. We reveal that targeting a positively charged cleft of DIMT1, remote from the catalytic site, weakens the binding of DIMT1 to rRNA and mislocalizes DIMT1 to the nucleoplasm, in contrast to the primarily nucleolar localization of wild-type DIMT1. Mechanistically, rRNA binding is required for DIMT1 to undergo liquid–liquid phase separation, which explains the distinct nucleoplasm localization of the rRNA binding-deficient DIMT1. Re-expression of wild-type or a catalytically inactive mutant E85A, but not the rRNA binding-deficient DIMT1, supports AML cell proliferation. This study provides a new strategy to target DIMT1-regulated AML proliferation via targeting this essential noncatalytic region.

[*Keywords*: RNA; cell proliferation; methyltransferase; phase separation]

Supplemental material is available for this article.

Received December 8, 2022; revised version accepted March 21, 2023.

Dimethyladenosine transferase 1 (DIMT1), a *S*-adenosyl methionine (SAM)-dependent methyltransferase, is an rRNA-modifying enzyme that participates in ribosome biogenesis (Chaker-Margot et al. 2015, 2017; Klinge and Woolford 2019). DIMT1 installs $N^{6,6}$-dimethyladenosine ($m_2{}^{6,6}A$) at the two adjacent adenosine sites A1850 and A1851, almost to 100% occupancy, in human 18*S* rRNA (Poldermans et al. 1980; O'Farrell et al. 2004; Mangat and Brown 2008; Tu et al. 2009; Boehringer et al. 2012). Previous studies reveal that the catalytic role of DIMT1 is important for stress response (Helser et al. 1971; Lafontaine et al. 1994; Tokuhisa et al. 1998; Wieckowski and Schiefelbein 2012) and is required for translational fidelity in bacterial and human cells (Shen et al. 2020). DIMT1 is located in the cell nucleolus where rRNA transcription, rRNA processing, and ribosome assembly take place (Zorbas et al. 2015). Specifically, DIMT1 participates in the late steps of 18*S* rRNA processing in a noncatalytical manner (Zorbas et al. 2015). Ablation of DIMT1 disrupts ribosome biogenesis and is lethal for human cells. Recently, we and others have shown that the catalytic activity of DIMT1 is not required for ribosome biogenesis (Zorbas et al. 2015; Shen et al. 2020, 2021). Thus, the function of DIMT1-mediated rRNA methylation and DIMT1's noncatalytic role in rRNA processing and ribosome biogenesis are decoupled.

Ribosome biogenesis is fundamentally important for cell growth and proliferation. Although ribosomes are ubiquitously expressed in all cell types, certain cell types (such as hematopoietic cells) are more affected by ribosomal defects than others (Mills and Green 2017). For instance, ribosomal defects are frequently seen in bone marrow failure, anemia, and hematopoietic malignancy. Mutations in ribosomal proteins RPL5 and RPL10 of the large ribosomal subunit have been implicated in T-cell acute lymphoblastic leukemia, and mutations in RPS15 of the small ribosomal subunit have been implicated in

[6]**These authors contributed equally to this work.**
Corresponding author: liufg@pennmedicine.upenn.edu
Article published online ahead of print. Article and publication date are online at http://www.genesdev.org/cgi/doi/10.1101/gad.350298.122.

chronic lymphocytic leukemia (Vlachos 2017). Early ribosome biogenesis occurs in the cell nucleolus where it represents a multilayered biomolecular condensate that is formed through a biophysical process called liquid–liquid phase separation (LLPS) (Feric et al. 2016). LLPS facilitates the initial steps of ribosome biogenesis and several other functions (Lafontaine et al. 2021). For instance, ribosomal proteins and rRNA-modifying enzymes such as the box C/D small nucleolar RNA-associated methyltransferase fibrillarin (FBL) and nucleophosmin (NPM1) reside in different layers in the nucleolus to facilitate rRNA synthesis and ribosomal subunit maturation steps (Amin et al. 2008). However, it is not known whether DIMT1 undergoes LLPS to the nucleolus to facilitate ribosome maturation or rRNA methylation. Since DIMT1 aids ribosome assembly in the nucleolus, understanding the mechanism by which DIMT1 localizes to the nucleolus may provide a new strategy to regulate its role in ribosome assembly.

Additionally, a diverse set of chemical modifications is found within rRNAs (Desrosiers et al. 1974, 1975; du Toit 2016; Gilbert et al. 2016; Lewis et al. 2017; Roundtree et al. 2017; Willyard 2017; Zhao et al. 2017). Critically, these modifications can dramatically alter rRNA structure, stability, and protein synthesis (Sloan et al. 2017). The functional significance of rRNA modifications is further evidenced by the fact that dysregulation of rRNA-modifying enzymes and snoRNAs (which guide rRNA-modifying enzymes to achieve substrate specificity) has been linked to a battery of human cancers, including hematopoietic malignancies (Narla and Ebert 2010; McMahon et al. 2015; Frye and Blanco 2016; Nachmani et al. 2019; Janin et al. 2020; Barros-Silva et al. 2021). DIMT1 is highly expressed in hematopoietic malignancies such as acute myeloid leukemia (AML) and multiple myeloma, and studies show that knockdown of DIMT1 leads to reduced tumorigenicity in myeloma (Zorbas et al. 2015; Ikeda et al. 2017, 2018; Janker et al. 2019). However, it is not known whether the catalytic role or the noncatalytic role of DIMT1 supports leukemia cell proliferation.

Here, we revealed a positively charged cleft that is remote from the catalytic center of DIMT1 and is essential for its RNA binding ability and function in ribosome biogenesis. Furthermore, this cleft is required for DIMT1 to undergo RNA-facilitated LLPS. Simultaneous mutation of those positively charged residues, which dampens the rRNA binding affinity of DIMT1, leads to aberrant nucleoplasm localization of DIMT1 and thus fails to support AML cell proliferation. The results also demonstrate that the noncatalytic role of DIMT1 instead of DIMT1-mediated rRNA methylation is important for AML cell proliferation.

Results

*DIMT1 depletion impairs 18*S *rRNA processing and AML cell proliferation*

Previous studies have suggested that DIMT1 is highly expressed in leukemia cells (Shen et al. 2021; https://depmap.org/portal/publications). The CERES score showed moderately higher dependency of leukemia cells on the *DIMT1* gene compared with all cancers (Supplemental Fig. S1A). To validate the requirement of DIMT1 in cancer cell proliferation, we performed a competition-based proliferation assay across a selection of cancer cell lines. We transduced single-guide RNAs (sgRNAs) targeting DIMT1, Rosa (a negative control), and PCNA (a positive control) coexpressed with the GFP marker into two AML cell lines and two solid tumor cells lines (Supplemental Fig. S1B). The resulting cell population was comprised of both transduced (GFP^+) and untransduced (GFP^+) cells, and the relative abundance of each population was tracked via flow cytometry. Unlike the effects of sgRosa, we found that cells expressing sgDIMT1 were rapidly outcompeted by nontransduced cells, as shown by flow cytometry-based tracking of GFP expression. Furthermore, the cellular competition results showed that the AML cell lines (MOLM-13C and MV4-11C) preferentially required DIMT1 for proliferation in comparison with solid tumor cell lines (Fig. 1A). The Western blot analyses confirmed the successful depletion of DIMT1 after 5 d of sgDIMT1 administration (Fig. 1B).

To further verify the essential function of DIMT1 and the on-target effect of our sgRNA, we ectopically expressed CRISPR-resistant WT-DIMT1 cDNA, which contains mutations at the sgRNA targeting site or an empty vector in leukemia cells (Fig. 1C). To achieve a proper expression level of our transgene, CRISPR-resistant WT-DIMT1, we transduced MOLM-13C cells at low multiplicity of infection (Supplemental Fig. S1C). Since exogenous DIMT1 had an mCherry tag separated by a P2A linker, we performed fluorescence-activated cell sorting (FACS) to enrich cells expressing exogenous DIMT1. Low multiplicity of infection following by cell sorting allowed us to achieve expression of exogenous DIMT1 close to its endogenous level (expression levels of exogenous WT-DIMT1 and E85A-DIMT1 are 2.69 ± 0.6 and 2.67 ± 0.4, while endogenous DIMT1 was normalized to 1). We then transfected the sgDIMT1 to target the endogenous DIMT1. As shown in Figure 1D, cells re-expressing WT-DIMT1 have rescued cell proliferation, but cells expressing the empty vector do not.

To dissect whether the enzymatic activity of DIMT1 is important for AML proliferation, we expressed CRISPR-resistant E85A-DIMT1 (catalytically inactive) (Shen et al. 2020) in MOLM-13C cells and performed the same assays as WT-DIMT1. As shown in Figure 1, D and E, cells re-expressing E85A-DIMT1 rescued MOLM-13C cell proliferation. We further investigated whether DIMT1 depletion influences 18*S* rRNA processing by performing Northern blots. We used DNA probes targeting ITS1 (Fig. 1F, top panel) and ITS2 (Fig. 1F, bottom panel) to quantify the levels of the rRNA precursors. The results suggest that DIMT1 depletion caused a substantial accumulation of 21*S* pre-RNA compared with the control cells (Fig. 1F,G).

DIMT1 depletion alters the expression and translation of transcripts involved in cell proliferation

To understand the impact of DIMT1 depletion on translation, we carried out ribosome profiling followed by high-

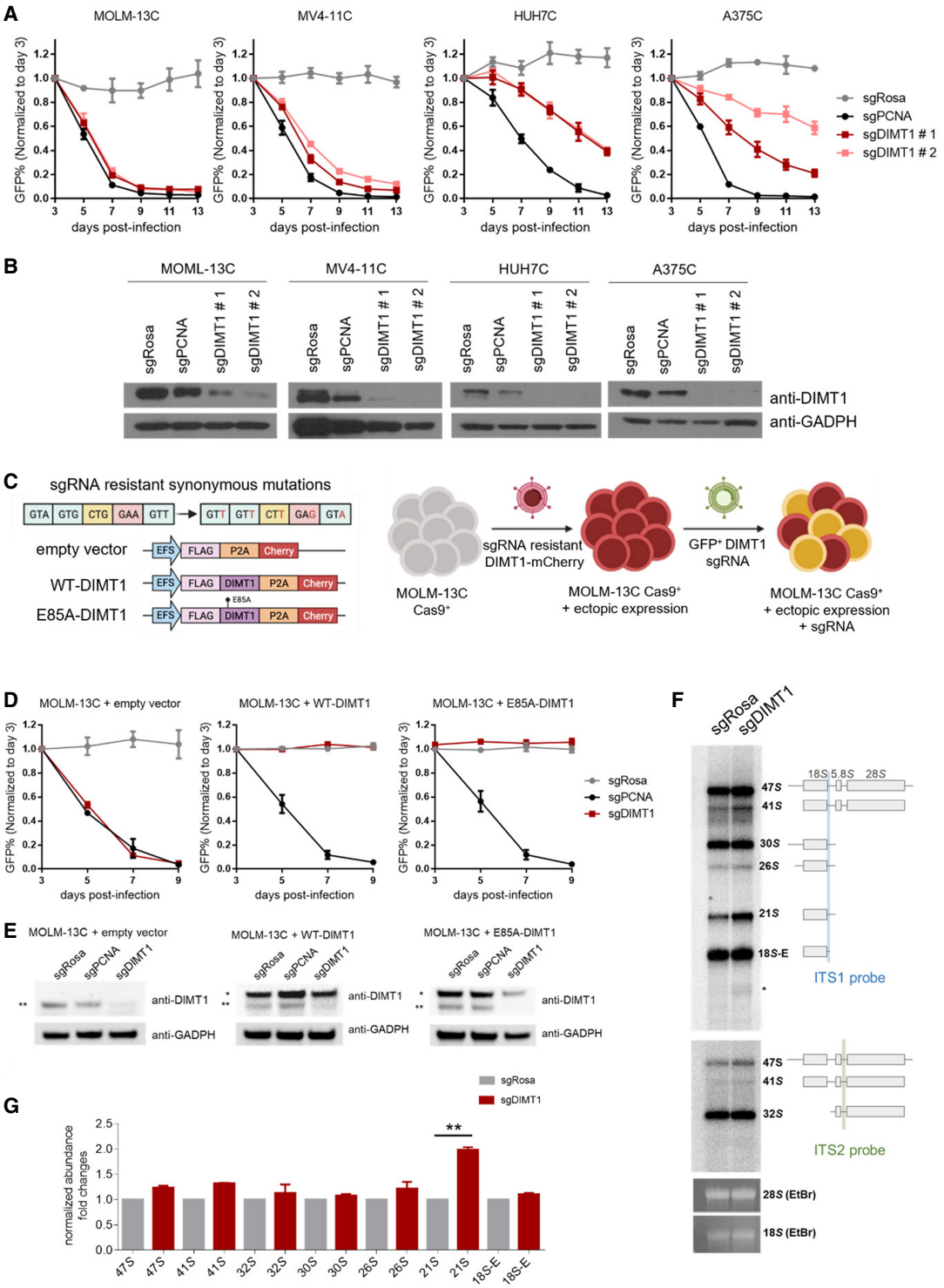

Figure 1. DIMT1 is essential for AML cell proliferation. (*A*) Competition-based proliferation assays performed in the indicated Cas9$^+$ cell lines. sgRNA$^+$ populations were monitored over time with a GFP coexpression marker. Plotted is the relative sgRNA$^+$ population normalized to the day 3 sgRNA$^+$ population over 13 d. sgRosa is the negative control, and sgPCNA is the positive control. (*B*) Western blots showing DIMT1 expression in cells transfected with the indicated sgRNAs on day 5 after infection. (*C*) Schematic of re-expressing WT-DIMT1, E85A-DIMT1, or empty vector in MOLM-13C cells. DIMT1 carries synonymous mutations, so it is not targeted by sgRNA of DIMT1. (*D*) Competition-based proliferation assay of MOLM-13C cells re-expressing WT-DIMT1, E85A-DIMT1, or an empty vector versus parental cells. (*E*) Western blots showing endogenous DIMT1 (indicated by two asterisks) and exogenous DIMT1 (indicated by one asterisk) expression in cells transfected with the indicated sgRNAs on day 5 after infection. (*F*) Northern blot analysis of rRNA precursors with total RNA extracted from MOLM13C cells transfected with negative control (sgRosa) or gRNA targeting DIMT1 (sgDIMT1). The detected pre-rRNA species are indicated at the *right* and schematized. The probes targeted ITS1 (*top* panel) and ITS2 (*bottom* panel). The mature 28*S* and 18*S* rRNAs were stained with ethidium bromide. (*G*) Quantification of rRNA precursors from *F*. The two-tailed *t*-test was used to calculate the *P*-value ($P = 0.0012$). Error bars represent mean ± SD.

throughput sequencing (Ribo-seq) in MOLM-13C cells transfected with sgRosa versus cells transfected with sgDIMT1. The principal component analysis is summarized in Supplemental Figure S2A, which shows the sequencing data of the ribosome-protected RNA (RIBO) and the input RNA (RNA) from DIMT1 depletion, as well as the control cells, separated well into sequencing group (RNA vs. RIBO) and treatment condition (sgRosa vs. sgDIMT1). The two biological replicates also cluster together, indicating the reliable quality of the sequencing data. First, we analyzed the differential gene expression. We found that DIMT1 depletion leads to significantly increased expression of 134 genes ($\log_2$ fold change > 1) (Fig. 2A; Supplemental Fig. S2B; Supplemental Table S1); gene ontology (GO) analysis indicated that the proteins encoded by these transcripts are mainly involved in the regulation of the immune response and cell adhesion (Fig. 2B). DIMT1 depletion also significantly decreases the expression of 18 genes ($\log_2$ fold change < −1); gene ontology (GO) analysis indicated that the proteins encoded by these

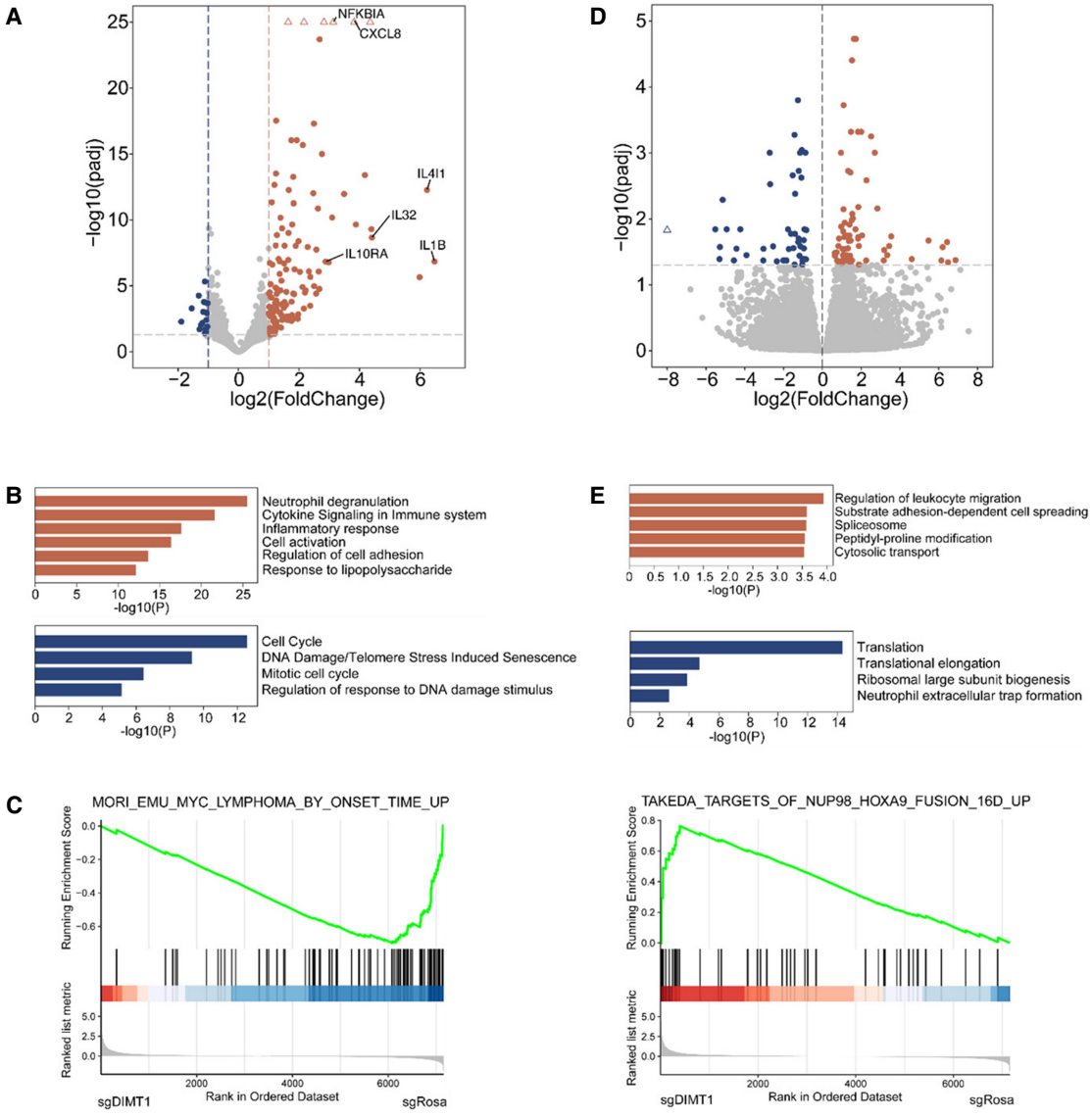

Figure 2. The effect of DIMT1 depletion on MOLM-13C cells. (*A*) A volcano plot showing the RNAs with differential expression levels in DIMT1-depleted versus control MOLM-13C cells. The significantly up-regulated (*P*adj < 0.05; $\log_2$ fold change > 1) transcripts are shown in orange, and the significantly down-regulated (*P*adj < 0.05; $\log_2$ fold change < −1) transcripts are shown in blue. (*B*) GO analysis of the significantly up-regulated and down-regulated transcripts that are shown in *A*. Transcripts with increased expression levels are in orange, and transcripts with decreased expression levels are in blue. (*C*) Gene set enrichment analysis (GSEA) of sequencing data presented in *B*. NUP98_HOXA9_fusion_up and MYC_lymphoma_up signatures were used. (*D*) A volcano plot showing the RNAs with differential translational efficiency in DIMT1-depleted versus control MOLM-13C cells. The significantly up-regulated (*P*adj < 0.05) genes are shown in orange, and the significantly down-regulated (*P*adj < 0.05) genes are shown in blue. (*E*) GO analysis of the differential transcripts in Figure 6D (below). Transcripts with increased translation efficiencies are in red, and transcripts with decreased translation efficiencies are in blue.

transcripts are mainly involved in the regulation of the cell cycle (Fig. 2A,B). Gene set enrichment analysis (GSEA) revealed that the MYC target gene signature and the HOX gene cluster signature are significantly altered upon DIMT1 depletion, indicating that dysregulation of DIMT1 may affect common cancer pathways and lead to a broad spectrum of cancers including leukemia (Fig. 2C). Next, we analyzed the translational efficiency difference between DIMT1-depleted cells and the control cells. As shown in Figure 2D, Supplemental Figure S2C, and Supplemental Table S2, 70 transcripts exhibited significantly increased translation efficiency upon DIMT1 depletion; these transcripts are mainly involved in the regulation of leukocyte migration and spliceosomes (Fig. 2E). Another 46 transcripts showed decreased ribosome occupancies upon DIMT1 depletion; these transcripts are mainly involved in the regulation of translation and ribosome biogenesis, which is consistent with the function of DIMT1 as a ribosome assembly factor (Fig. 2D,E).

A cleft in DIMT1 consisting of five positively charged residues is important for its RNA binding

DIMT1 associates with preribosomes at the early steps of 18*S* rRNA processing and 40*S* small subunit assembly in the nucleolus (Zorbas et al. 2015). Since the catalytic activity of DIMT1 is not required for AML proliferation (Fig. 1D), we next investigated whether we could impede DIMT1 joining ribosome assembly to reduce AML proliferation. We analyzed the residues in DIMT1 that contact 18*S* rRNA. As shown in the structure of DIMT1 (PDB 7MQA) (Fig. 3A,B; Shen et al. 2021), there is a positively charged cleft between the N-terminal domain and the C-terminal domain of DIMT1 that contacts helix 45 in 18*S* rRNA. There are five positively charged residues—including Arg162 and Arg174 in the N-terminal domain and Arg228, Lys253, and Arg256 in the C-terminal domain of DIMT1—that are particularly noteworthy for their potential rRNA binding ability (Fig. 3B). We asked whether these residues contribute to DIMT1's RNA binding and processing of 18*S* rRNA.

To investigate whether these positively charged residues in the cleft are important for DIMT1's binding of 18*S* rRNA, we constructed a DIMT1 variant that contains five mutations inducing R162A, R174A, R228A, K253A, and R256A, which we refer to as 5mutA-DIMT1. We further expressed and purified full-length recombinant WT-DIMT1 and 5mutA-DIMT1 proteins (Supplemental Fig. S3A) and performed differential scanning fluorimetry experiments. The results suggest that WT-DIMT1 and 5mutA-DIMT1 are both well-folded proteins and share similar melting temperatures (Fig. 3C,D), as improperly folded, aggregated, or denatured proteins would typically present high background at low temperatures of a melting curve (Gao et al. 2020). Additionally, as shown in Supplemental Figure S3B, the AlphaFold-predicted structure of 5mutA-DIMT1 superimposed very well with the structure of WT-DIMT1 (with a root mean square deviation of atomic positions = 0.177 Å). Collectively, these results suggest that 5mutA does not lead to major structural changes in WT-DIMT1.

We then performed electrophoretic mobility shift assays (EMSAs) to compare the RNA binding affinities of WT-DIMT1 and 5mutA-DIMT1. We used a synthetic RNA probe with carboxyfluorescein at the 5′ end (5′ FAM). This probe bears the same local structure as the two modification sites of DIMT1 in helix 45 of 18*S* rRNA (Supplemental Fig. S3C). As shown in Figure 3, E and F, the binding affinity of 5mutA-DIMT1 to the RNA probe significantly decreases in comparison with WT-DIMT1. We determined K_{half}, which represents the concentration of an enzyme reaching half maximal binding. The K_{half} decreases from 1.2 µM protein for WT-DIMT1 to 3.9 µM for 5mutA-DIMT1. Next, we performed in vitro methylation assays using WT-DIMT1 or 5mutA-DIMT1 in the presence or absence of SAM. The substrate RNA probe was of the same sequence (but no 5′ FAM) as used in the EMSAs. The liquid chromatography triple-quadrupole mass spectrometry (LC-MS/MS) quantification results show that WT-DIMT1 effectively installs $m_2^{6,6}A$ in this RNA probe, while only background level of $m_2^{6,6}A$ can be detected in the reaction using 5mutA-DIMT1 (Supplemental Fig. S3D,E). These results suggest that 5mutA-DIMT1 is weaker than WT-DIMT1 in methylation installation because of the weaker RNA binding ability.

rRNA binding is a determinant for the nucleolar localization of DIMT1

Since *DIMT1* is an essential gene, we used a *DIMT1*$^{+/-}$ heterozygous HEK293T cell line that we established previously (Shen et al. 2020) to study the cellular localization of WT DIMT1, E85A-DIMT1 (a catalytically inactive variant), and 5mutA-DIMT1 in cells. We reconstituted empty vector, WT-DIMT1, E85A-DIMT1, and 5mutA-DIMT1 in this *DIMT1*$^{+/-}$ heterozygous cell line (Shen et al. 2020). Exogenous FLAG-tagged WT-DIMT1, FLAG-tagged E85A-DIMT1, and FLAG-tagged 5mutA-DIMT1 express comparable levels in *DIMT1*$^{+/-}$ heterozygous cells (Supplemental Fig. S3F). The immunofluorescence imaging results show that 5mutA-DIMT1 predominantly localizes to the nucleoplasm, while WT-DIMT1 and E85A-DIMT1 both colocalize well with fibrillarin in the nucleolus (Fig. 3G). Similarly, MOLM-13C cells expressing WT-DIMT1-mClover or E85A-DIMT1-mClover, but not 5mutA-DIMT1-mClover, localize in the nucleolus (Supplemental Fig. S3G). The results suggest that rRNA binding may be essential for the primary localization of DIMT1 in the nucleolus, while the enzymatic activity is not required for its localization. DIMT1 not only interacts with 18*S* rRNA but also associates with two other ribosome assembly factors (BMS1 and DHX37), as shown in the small subunit processome structure (PDB 7MQ9) (Singh et al. 2021). Immunostaining analyses of MOLM-13C cells that express only exogenous WT-DIMT1 or 5mutA-DIMT1 shows that BMS1 remains in the nucleolus in both WT-DIMT1- and 5mutA-DIMT1-expressing cells (Supplemental Fig. S3H). These data suggest that the RNA binding deficiency of

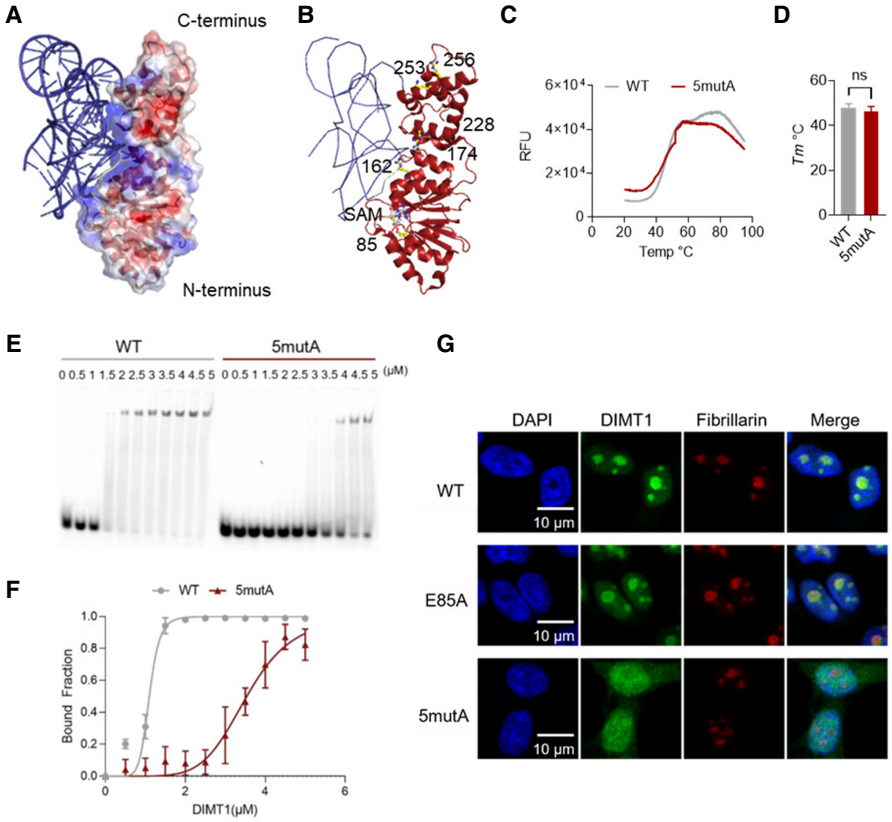

Figure 3. 5mutA-DIMT1 presents weaker RNA binding affinity. (*A*) The electrostatic surface of DIMT1 is shown to reveal the details of the RNA binding surface (PDB 7MQA). (*B*) Five positively charged residues, glutamate 85, and SAM are depicted as stick and ball structures. (*C*) Differential scanning fluorometry (DSF) melting curves showing the relative fluorescence units with increasing temperature. (*D*) The fluorescence is a product of SYPRO Orange dye, which resides on hydrophobic residues of exposed residues of WT-DIMT1 and 5mutA-DIMT1. The steady increase in fluorescence is due to the unfolding of the protein with increased temperature and the subsequent binding of the SYPRO Orange dye. (*E*) EMSA experiments show WT-DIMT1 and 5mutA-DIMT1 binding to the RNA probe. (*F*) RNA binding was plotted using the equation detailed in the Materials and Methods. WT-DIMT1 and 5mutA-DIMT1 at the indicated concentrations and 5′ FAM-labeled RNA probe at 1 µM were used. (*G*) Representative fluorescence microscopy images of FLAG-tagged WT-DIMT1-mClover, E85A-DIMT1-mClover, and 5mutA-DIMT1-mClover in *DIMT1*$^{+/-}$ HEK293T cells. The nucleoli were stained with an antifibrillarin antibody as a marker (red), and the nuclei were stained with a NuclearMask dye (blue). Scale bar, 10 µm.

DIMT1 does not significantly impact the nucleolar localization of its associated proteins.

We further quantified the cellular $m_2^{6,6}A$ levels in 18*S* rRNA using LC-MS/MS. The results showed that the levels of $m_2^{6,6}A$ in 18*S* rRNA are significantly lower in E85A-DIMT1 cells compared with WT-DIMT1, 5mutA-DIMT1, and empty vector-expressing *DIMT1*$^{+/-}$ cells (Supplemental Fig. S3I). We previously showed that *DIMT1*$^{+/-}$ heterozygous cells do not have lower $m_2^{6,6}A$ levels in 18*S* rRNA compared with the wild-type HEK293T cells; however, exogenous E85A-DIMT1 competes with endogenous WT-DIMT1 in binding to 18*S* rRNA and thus leads to lower $m_2^{6,6}A$ levels in 18*S* rRNA (Shen et al. 2020). In contrast, 5mutA-DIMT1 cells have fully modified 18*S* rRNA, similar to the empty vector-expressing *DIMT1*$^{+/-}$ cells, suggesting that exogenous 5mutA-DIMT1 cannot compete with endogenous WT-DIMT1 in binding to 18*S* rRNA (Supplemental Fig. S3I). These results suggest that the cleft region consisting of the five positively charged residues are critical for RNA binding and catalysis by DIMT1 in vitro and in cells.

rRNA binding is indispensable for DIMT1 undergoing phase separation

What is the molecular mechanism underlying the nucleoplasmic localization of 5mutA-DIMT1? We first suspected that 5mutA-DIMT1 might disturb the nucleolar leading sequence (NoLS) in DIMT1. NoLS detector predicted that residues 1–26 harbored the nucleolar leading sequence (Supplemental Fig. S4A,B). We fused the predicted NoLS to the N terminus of mClover. The results showed an enrichment of NoLS-mClover in the nucleolus compared with expressing mClover alone (Supplemental Fig. S4C). Next, we truncated the first 26 residues and constructed the ΔNoLS-DIMT1. The immunofluorescent imaging revealed that ΔNoLS-DIMT1 still remains localized to the nucleolus (Supplemental Fig. S4D). These studies suggest that the N-terminal segment of DIMT1 (a putative NoLS) does not play a leading role in DIMT1's nucleolar localization.

The first 26 residues of DIMT1 are not visible in previous crystal structures despite its presence in the

crystallized construct (Shen et al. 2020), which is likely due to its disordered nature (Supplemental Fig. S4E). We used AlphaFold software to predict the structures of WT-DIMT1 (with high per-residue confidence score [pLLDT] over 90% of the amino acid sequence) (Supplemental Fig. S5A). The first 26 residues are predicted to adopt a helical secondary structure with a low pLLDT score <50% (Supplemental Fig. S5B,C) and are far from the five positively charged cleft residues mutated in this study. Since the nucleolus represents a multilayered biomolecular condensate whose formation by LLPS facilitates ribosome biogenesis and other functions (Lafontaine et al. 2021), we wondered whether DIMT1 undergoes LLPS and whether this biophysical process is important for its nucleolar localization. Thus, we performed in vitro droplet assays using purified DIMT1-mClover (Supplemental Fig. S5D). The results showed that WT-DIMT1 alone does not form droplets in vitro using 12.5 µM protein and a series of salt concentrations. Remarkably, the addition of total RNA extracted from HeLa cells promotes the formation of droplets of WT-DIMT1 (Fig. 4A). As the RNA concentration increases (16.7–100 ng/µL), the apparent volume of the condensed phase (roughly indicated by the total droplet area in each image) increases. The most evident round droplets of WT-DIMT1 with RNA were formed using 200 mM NaCl with 100 ng/µL total RNA, since increasing NaCl concentrations to 400 mM and beyond diminished the droplet formation. At identical protein, RNA, and salt concentrations, 5mutA-DIMT1 presents significantly lower, nearly nondetectable droplet formation compared with WT-DIMT1 (Fig. 4B). At the optimal condensation formation condition for WT-DIMT1 (200 mM NaCl with 100 ng/µL total RNA), the condensation intensity of 5mutA-DIMT1 is nearly undetectable using the same exposure settings and equal intensity as those used for WT-DIMT1 (Fig. 5A,B).

We next studied the dynamics of the DIMT1-RNA droplets using fluorescent recovery after photobleaching (FRAP). We measured the recovery halftime and mobile fraction of the DIMT1-RNA droplets by using a one-phase association nonlinear regression curve. The recovery halftime for WT-DIMT1-RNA droplets is ~4.9 sec, while it is ~9.2 sec for nucleoplasmic 5mutA-DIMT1 (Fig. 5C,D). We observed that WT-DIMT1 and 5mutA-DIMT1 have mobile fractions of 62% and 30.8%, respectively (Fig. 5E). Together, these results suggest that RNA binding is essential for DIMT1 to undergo LLPS in vitro.

To assess whether DIMT1 undergoes LLPS in the cell nucleolus, we expressed DIMT1-mClover (both WT and E85A) in HEK293T *DIMT1*$^{+/-}$ cells. As shown in Figure 5F, the mClover tag on WT and E85A does not disturb the nucleolar localization of the proteins. We then performed FRAP to determine the dynamics of nucleolar WT-DIMT1. FRAP experiments performed on live HEK293T cells expressing WT-DIMT1 or 5mutA-DIMT1 reveal that the average recovery halftime of WT-DIMT1 nucleolar puncta is 0.8 sec, which is noticeably faster than the 1.68-sec recovery halftime of nucleoplasm 5mutA-DIMT1 (Fig. 5F). These results suggest that WT-DIMT1 undergoes LLPS in vitro and in cells, and rRNA binding-promoted LLPS of WT-DIMT1 is a possible driving force for the nucleolar localization of DIMT1.

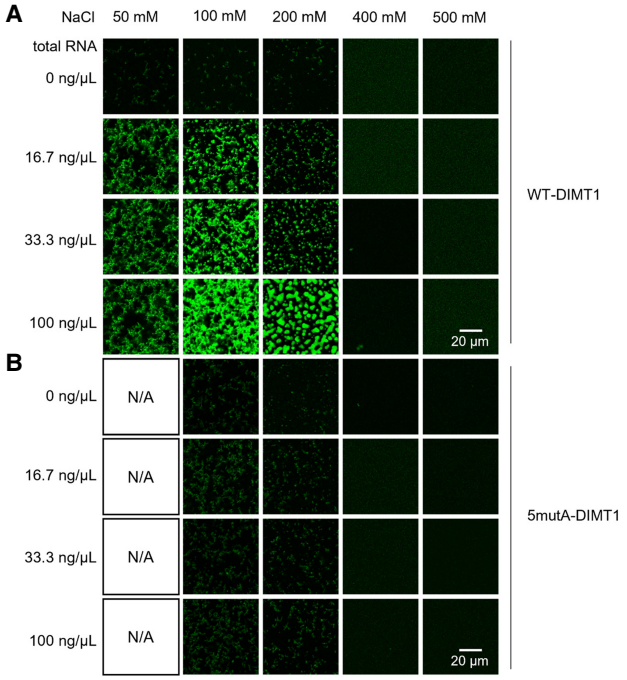

Figure 4. WT-DIMT1 but not 5mutA-DIMT1 forms liquid condensates in vitro. In vitro droplet formation of 10 µM recombinant WT-DIMT1-mClover (*A*) and 5mutA-DIMT1-mClover (*B*) in the presence of the indicated concentrations of total RNA in the buffer with the indicated salt concentrations. Scale bar, 20 µm.

The noncatalytic rRNA binding ability of DIMT1 is critical for cell proliferation

To assess the significance of the nucleolar localization of DIMT1 in promoting cell proliferation, we performed competition-based proliferation assays using CRISPR-resistant WT-DIMT1, 5mutA-DIMT1, and ΔNoLS-DIMT1 in MOLM-13C cells. The Western blot analyses suggest that 5mutA-DIMT1 was expressed close to the endogenous level of DIMT1 in MOLM13C cells (Supplemental Fig. S5A). As shown in Figure 6A, MOLM-13C cells re-expressing 5mutA-DIMT1 showed the same proliferation as cells re-expressing an empty vector—both presenting significant decreases in cell proliferation compared with cells re-expressing wild-type DIMT1. In contrast, WT-DIMT1- and ΔNoLS-DIMT1-expressing cells do not present decreased cell proliferation after transduction of the sgDIMT1 targeting endogenous DIMT1 (Fig. 6A). Pre-rRNA processing in MOLM-13C cells expressing 5mutA-DIMT1, WT-DIMT1, and E85A-DIMT1 after transduction with sgRosa or sgDIMT1 was analyzed by using Northern blotting (Fig. 6B). Depletion of endogenous DIMT1 caused significant accumulation of the 21*S* precursor only in 5mutA-DIMT1-expressing, but not in WT-DIMT1- and E85A-DIMT1-expressing, cells. These results indicate that only WT-DIMT1 and E85A-DIMT1, but not the RNA binding-

deficient 5mutA-DIMT1, are able support 18*S* rRNA processing. Polysome profiling of MOLM-13C cells expressing 5mutA-DIMT1, WT-DIMT1, and E85A-DIMT1 with the endogenous DIMT1 depleted demonstrated decreased levels of polysomes only in 5mutA-DIMT1 cells (Fig. 6C). To determine the translational status of the top five mRNA targets identified by Ribo-seq in DIMT1 depletion compared with the control, we performed qRT-PCR on RNA isolated from the light and heavy fractions of the polysome profiles. The results showed that the five mRNAs that presented increased ribosome occupancies upon DIMT1 depletion in Ribo-seq are enriched in the heavy fractions of the gradients in cells expressing 5mutA-DIMT1 but not WT-DIMT1 or E85A-DIMT1 (Fig. 6D). Altogether, these results consistently demonstrate that RNA binding-facilitated nucleolar localization, but not the methyltransferase activity, of DIMT1 is essential for ribosome biogenesis to support AML proliferation.

Discussion

Previous studies have emphasized that dysregulation of ribosome assembly results in distinct types of human diseases, including cancers. However, there is limited knowledge about the underlying mechanism by which ribosome assembly factors and enzymes lead to these diseases. Here we investigated the noncatalytic role of ribosome assembly factor DIMT1 in cell proliferation. The results of competition-based proliferation assays demonstrated that AML cell lines show higher sensitivity to DIMT1 loss compared with the tested solid tumor cell lines. Ribosome profiling of AML cells upon DIMT1 depletion revealed subsets of dysregulated transcripts, including MYC and HOX mRNAs implicated in variety of different cancers, suggesting that DIMT1 affects common cancer pathways and may impact a broad spectrum of cancers including leukemia.

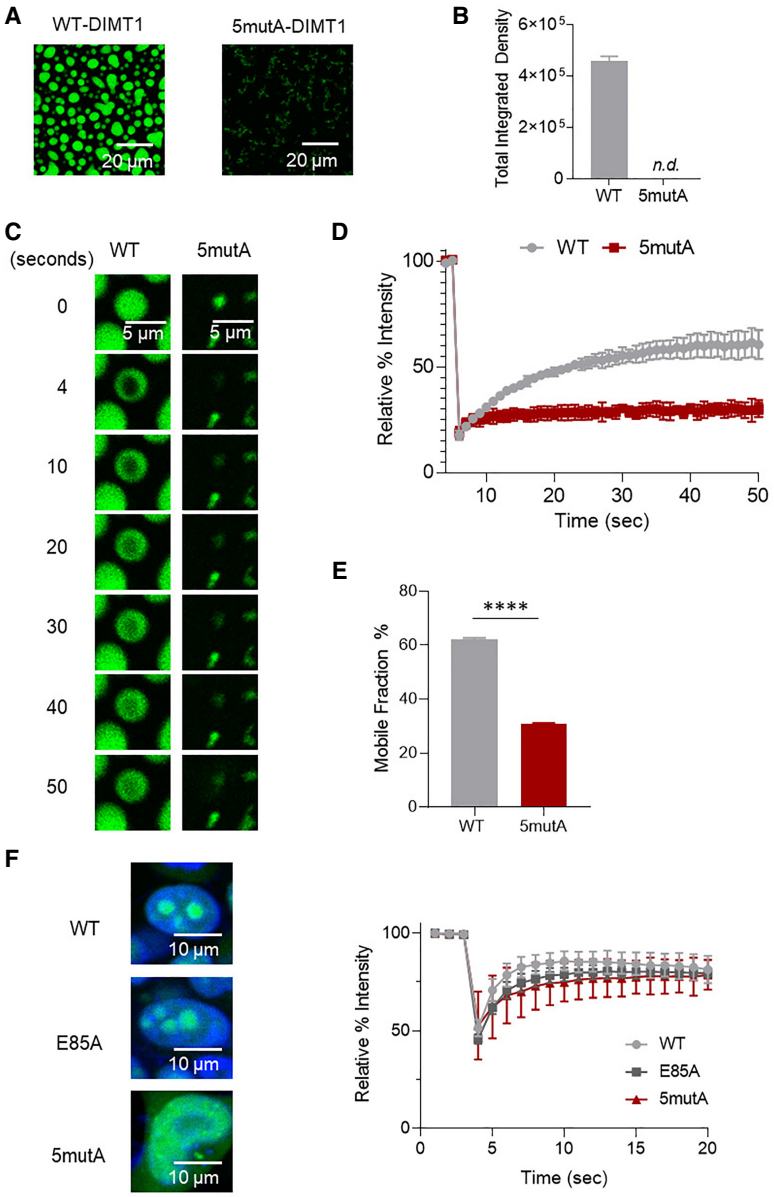

Figure 5. WT-DIMT1, but not 5mutA-DIMT1, forms liquid condensates. (*A*) In vitro droplet formation of 10 µM recombinant WT-DIMT1-mClover and 5mutA-DIMT1-mClover in the presence of 100 ng/µL total RNA and 200 mM NaCl. Scale bar, 20 µm. (*B*) Quantification of the total integrated intensity of WT-DIMT1-RNA condensation and 5mutA-DIMT1-RNA condensation in Figure 4A. (*C*) Time-lapse images of 12.5 µM mClover-WT-DIMT1 and 10 µM 5mutA-DIMT1-mClover droplets from in vitro FRAP experiments. Droplets were formed in the presence of 100 ng/µL total RNA and 200 mM NaCl. The FRAP experiments were performed using the same conditions for WT-DIMT1-mClover and 5mutA-DIMT1-mClover. Scale bar, 5 µm. (*D*) FRAP curves for the in vitro droplets of mClover-WT-DIMT1 (gray) and mClover-5mutA-DIMT1 (maroon). The traces of the FRAP data represent mean ± SEM. $n = 3$ from three independent experiments. (*E*) The mobile fractions from *D* show that 5mutA-DIMT1 has a significantly slower recovery phase compared with WT-DIMT1. The two-tailed *t*-test was used to calculate the *P*-value. (****) $P < 0.0001$. (*F*) Images and FRAP analysis of recovery curves for WT-DIMT1-mClover (gray), E85A-DIMT1-mClover (dark gray), and 5mutA-DIMT1-mClover (maroon) in *DIMT1*$^{+/-}$ HEK293T cells. The fast fluorescence recovery plots indicate the liquid-like nature of the puncta of WT-DIMT1 and E85A-DIMT1 but not 5mutA-DIMT1. The traces of the FRAP data represent mean ± SEM. $n = 20$ independent experiments from three biologically independent experiments.

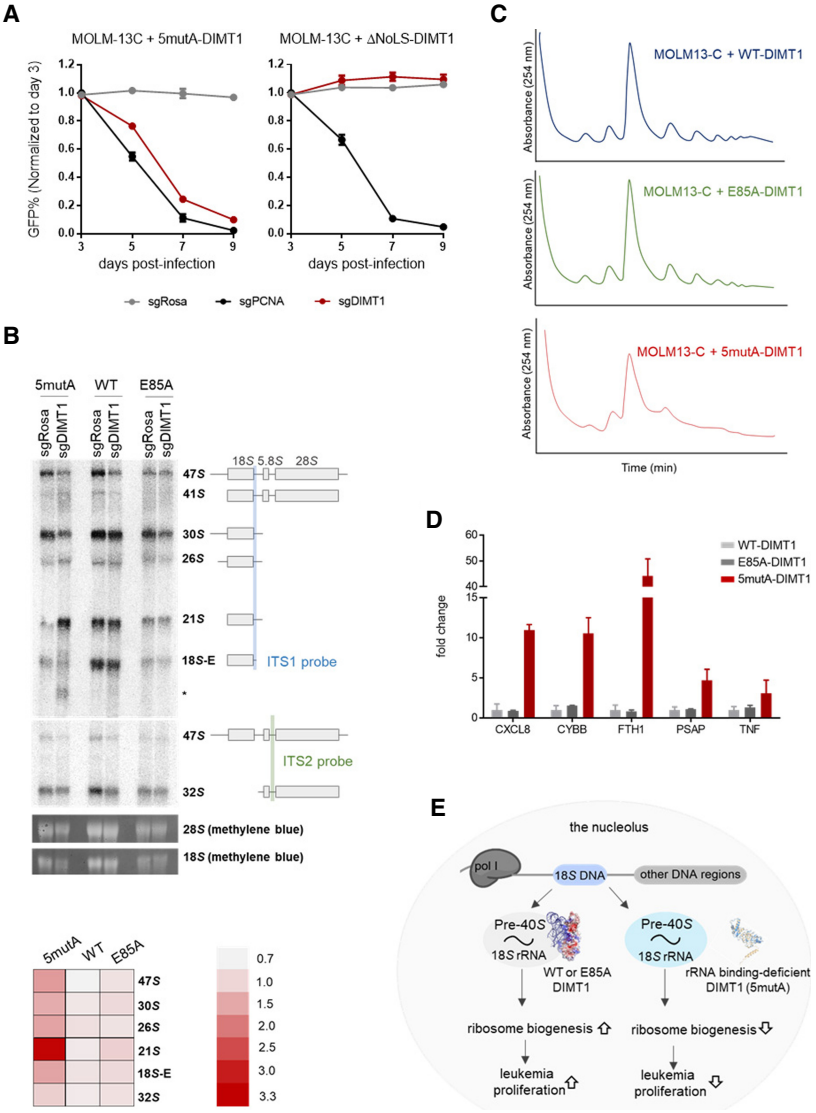

Figure 6. The RNA binding region, but not the catalytic activity, of DIMT1 is required for cell proliferation. (*A*) Competition-based proliferation assay of MOLM-13C cells re-expressing sgRNA-resistant 5mutA-DIMT1 (*left*) and ΔNoLS-DIMT1 (*right*). Cells were transduced with the indicated sgRNAs (sgRosa as a negative control, sgPCNA as a positive control, and sgDIMT1). (*B*, *top* panel) Representative Northern blots showing pre-rRNA processing in MOLM-13C cells re-expressing sgRNA-resistant 5mutA-DIMT1, WT-DIMT1, and E85A-DIMT1 after transduction with the indicated sgRNAs. Northern blot analyses were performed using two probes targeting ITS1 and ITS2. The detected pre-rRNA species are indicated at the *right* and schematized. (*Bottom* panel) The abundance of rRNA precursors of two biological replicates was quantified with a phosphorimager and converted into a heat map. The heat map shows the abundance of each pre-rRNA species in sgDIMT1-infected cells compared with the abundance of the same pre-rRNAs in cells infected with sgRosa. (*C*) Polysome profiles of MOLM-13C cells expressing exogenous WT/E85A/5mutA-DIMT1 after knockout of endogenous DIMT1. (*D*) Results of the qRT-PCR of RNA extracted from the light or heavy fractions of the polysome profiles shown in *C* performed in two biological replicates. The *Y*-axis represents the abundance of mRNA in the heavy fraction relative to in the light fraction. The fold change values of the relative mRNA abundance in WT-DIMT1 cells were normalized to 1. (*E*) Schematic illustration of a positively charged cleft in DIMT1 supports 40*S* small subunit assembly and leukemia proliferation. The empty arrows indicate up-regulation (stimulating) or down-regulation (inhibiting) of the proliferation.

Using a catalytically dead DIMT1 mutant, we showed that MOLM-13C cells rely on DIMT1 not for its catalytic activity but for its ability to bind to 18*S* RNA for its nucleolar localization and function (Fig. 6C). Of note, our study of 5mutA-DIMT1 and ΔNoLS-DIMT1 reveals that the rRNA binding but not the predicted nucleolar leading sequence is the driving force for nucleolar localization. Taken together, our study of a positively charged cleft in DIMT1 provides insight into the vital role that rRNA binding plays in the nucleolar phase separation and functions of DIMT1. This discovery opens new avenues to studying other ribosome assembly factors and their connections to cancers.

rRNA binding affinity but not the putative nucleolar localization sequence is important for the nucleolar localization of DIMT1

The nucleolus is the hallmark of nuclear compartmentalization and plays a primary role in rRNA synthesis and ribosome assembly. DIMT1 localizes in the nucleolar compartment. Previous studies show that short protein sequences with a minimum of five basic amino acids (often lysine and arginine residues) are termed nucleolar localization sequences (NoLSs) (Martin et al. 2015). Nuclear proteins without nucleolar function are often less concentrated or completely excluded from the nucleoli, while nucleolar proteins are highly enriched in this nuclear compartment. Although NoLSs have been identified in nucleolar proteins, it remains unclear which properties or requirements of such proteins are essential for accumulation in the nucleoli. We noticed that DIMT1 contains a predicted NoLS at the N terminus of the protein (Supplemental Fig. S4A). However, deleting this region did not alter the nucleolar localization of DIMT1. In contrast, mutations of a basic RNA binding cleft that do not disturb the predicted NoLSs are responsible for modulating the nucleolar localization of DIMT1, which highlights the role of rRNA binding in cellular localization.

RNA-promoted phase separation is a possible mechanism for DIMT1 localization in the nucleolus

The nucleolus is the most prominent nuclear compartment and is formed by liquid–liquid phase separation of proteins and protein/RNA complexes. This multilayered subcellular compartment performs a host of diverse roles in a highly organized manner. In this study, we investigated whether DIMT1 undergoes liquid–liquid phase separation in vitro and inside cells. Our results suggest that RNA binding promotes in vitro droplet formation of WT-DIMT1 but not 5mutA-DIMT1. Additionally, WT-DIMT1 presents a liquid condensation property in the nucleolus. These results suggest that RNA-promoted LLPS is a possible mechanism for DIMT1 localizing in the nucleolus. However, this study does not exclude the possibility that 18*S* rRNA binding facilitates the nucleolar localization of DIMT1 regardless of its LLPS status.

The localization of proteins and RNAs to the nucleolus is critical for a host of biological events (Lafontaine et al. 2021). The localization or exclusion of proteins from the nucleolus can dramatically change in response to cellular stimuli and reorganization during cell cycle progression. DIMT1 is an indispensable assembly factor in 18*S* rRNA processing and 40*S* subunit assembly. Thus, the function of DIMT1 may be better facilitated by its high concentration in the nucleolus. Additionally, DIMT1-mediated $m_2^{6,6}A$ occurs at two adjacent sites in 18*S* rRNA at nearly 100% occupancy. We predict that enriched DIMT1 in the nucleolus might be indispensable for its catalysis. Although DIMT1-mediated $m_2^{6,6}A$ is not required for the proliferation of MOLM-13C cells, the double methylation does play a role in other cellular aspects such as cell differentiation, especially since the loss of DIMT1-mediated $m_2^{6,6}A$ sensitizes living organisms to stress conditions and decreases translational fidelity (Helser et al. 1971; Lafontaine et al. 1994; Tokuhisa et al. 1998; Wieckowski and Schiefelbein 2012).

The rRNA cleft identified in this study is an Achilles' heel of DIMT1

DIMT1 is a common essential gene that is indispensable for ribosome biogenesis. However, our results suggest that certain cell types such as AML cells are more sensitive to DIMT1 deficiency (Fig. 1A). In our previous study (Shen et al. 2021), we observed that *DIMT1*$^{+/-}$ HEK293T cells expressing E85A-DIMT1 have reduced translation and cell proliferation compared with *DIMT1*$^{+/-}$ HEK293T cells expressing WT-DIMT1. However, E85A-DIMT1-expressing MOLM-13C cells have cell proliferation indistinguishable from WT-DIMT1 cells. It is not known whether E85A-DIMT1 MOLM-13C cells have translational status comparable with WT-DIMT1 MOLM-13C cells. We reasoned that the cell type specificity might contribute to the different requirements of DIMT1's catalytic role in the cell proliferation of HEK293T and MOLM-13C cells. Additionally, the *DIMT1*$^{+/-}$ HEK293T system still contains the remaining endogenous DIMT1, which is different than the MOLM-13C system that expresses E85A-DIMT1 before complete ablation of endogenous DIMT1.

Since we show that DIMT1 supports MOLM-13C cell proliferation through promoting rRNA processing and ribosome biogenesis, methods to regulate DIMT1's noncatalytic role in ribosome assembly could be further pursued. Given that the data in this study show that the RNA binding cleft is linked to DIMT1's nucleolar localization and function (Figs. 3G, 6), it may be a new therapeutic site for targeting DIMT1 in rapidly dividing cells, such as in AML proliferation. Identifying this indispensable role of an rRNA binding cleft remote from DIMT1's catalytic site is important and potentially inspiring because there are several other rRNA-modifying enzymes and rRNA binding proteins that also function as assembly factors in preribosomal complexes in the nucleolus. Tackling the RNA binding ability of these similar rRNA-modifying enzymes and rRNA binding proteins may provide a new therapeutic avenue for ribosomopathies.

In summary, this study describes an RNA binding cleft of DIMT1 and uncovers its function in controlling DIMT1's cellular localization and role in promoting cell proliferation. The findings detailed in this report open new avenues for studying ribosome assembly factors and introduce a potential therapeutic target in treating ribosome defects such as those in AML and other human disorders related to ribosomal defects.

Materials and methods

Mammalian cell culture, lentivirus production, and transduction

HEK293T, HUH7C, and A375C cells were cultured in DMEM + GlutaMAX (Gibco 11995065) with 10% FBS (Gibco 26140-079) and 1% penicillin/streptomycin (Corning 30-002-CI) in a humidified incubator with 5% CO_2 at 37°C. MOLM-13C and MV4-11C cells were cultured in RPMI (Gibco 22400-089) supplemented with 10% FCS and 1% penicillin/streptomycin.

For lentivirus production, HEK293T cells in a 10-cm plate at 90%–100% confluency were transfected with 10 µg of plasmids of interest, 5 µg of VSV-G plasmid, and 7.5 µg of psPAX2 plasmid using 80 µL of 1 mg/mL polyethylenimine (Polysciences 25000) in 500 µL of Opti-MEM (Gibco 31985062). The media was changed with 6 mL of fresh DMEM 6–8 h after transfection. Lentivirus was collected twice a day for the next 3 d after transfection. Collected virus was pooled together, filtered with a 0.45-µm PVDF filter (Millipore), and stored at −80°C in small aliquots for long-term use.

For viral transduction, cells of interest were transduced with lentivirus using 4 µg/mL polybrene (Sigma H9268) and centrifuged at 650*g* for 25 min at room temperature. The transduced cells were incubated overnight at 37°C, and media was replaced 15 h after infection.

Construction of stable cell lines

HEK293T stable cell lines were generated in HEK293T *DIMT1*$^{+/-}$ heterozygous background using pPB vector as previously described (Shen et al. 2020). Transfection was performed at 60% cell confluency using Lipofectamine 2000 (Invitrogen 11668019). Twenty-four hours after transfection, the cells were selected under 2 µg/mL puromycin for 2 wk. During the selection period, cells were resuspended every 2 d with fresh DMEM supplemented with 10% FBS and 2 µg/mL puromycin. The stable

overexpression was confirmed by Western blotting using an anti-FLAG antibody (Thermo MA1-91878-HRP).

To create MOLM-13C stable cell lines, MOLM-13C cells were transduced with WT-CRISPR-resistant and E85A-CRISPR-resistant DIMT1 followed by a P2A-linked mCherry. Transduced MOLM-13C cells containing ~30% mCherry-positive cells were sorted and collected using a FACS MoFlo Astrios cell sorter (Beckman).

Plasmid constructs

For DIMT1 and recombinant DIMT1-mClover protein expression, DIMT1 mutations were introduced through site-directed mutagenesis PCR into a pET-28a vector to generate DIMT1 5mutA. DIMT1-mClover constructs were introduced into pET-28a through fusion PCR to generate a DIMT1-mClover insert. This was used to generate DIMT1-WT-pET-28a-mClover, DIMT1-E85A-pET-28a-mClover DIMT1, and 5mutA-pET-28a-mClover vectors.

For transfection and establishment of HEK293T stable cell lines, DIMT1-5mutA-pPB vector was generated by subcloning a 5mutA insert from an existing DIMT1-5mutA-pET-28a vector. Similarly, DIMT1-mClover constructs were subcloned out of pET-28a-mClover vectors into pPB vectors to generate DIMT1-pPB-mClover vectors. The ΔNoLS was generated by truncating amino acids 1–26 and insertion into pPB and pPB-mClover vectors.

To generate sgRNA-encoding plasmids, sense and antisense DNA oligos were annealed and ligated into a BsmbI-digested LRG2.1 expressing GFP (Addgene 108098).

To generate the CRISPR-resistant DIMT1 mutant, the following base substitutions were introduced into the DIMT1 cDNA by PCR mutagenesis: A177→T, G180→T, G183→T, A186→G, and T189→A. CRISPR-resistant DIMT1 was cloned into Lenti Cherry vector using the In-Fusion cloning system (Takarabio 638943). Generated vectors encoded N-terminal FLAG-tagged CRISPR-resistant WT-DIMT1 and E85A-DIMT1, which were followed by P2A-linked mCherry.

All plasmids were validated through Sanger sequencing.

Protein purification

pET-28a vectors were transformed into *Escherichia coli* BL21 (DE3 C2527H) for purification. Bacteria were grown at 37°C until an optical absorbance at 600 nm between 0.6–0.8 was achieved, at which point protein expression was induced by the addition of IPTG at 1 mM final concentration. After overnight growth at 16°C, cells were collected and lysed using lysis buffer (25 mM Tris-HCl at pH 7.5, 500 mM NaCl). Cell lysate was centrifuged at 11,000 rpm for 30 min at 4°C, and the supernatant was then loaded onto a Ni-affinity chromatography column (GE Healthcare), which was pre-equilibrated using the lysis buffer. The loaded column was washed with 100 mL of wash buffer (50 mM imidazole in lysis buffer) before the bound protein was eluted with elution buffer (500 mM imidazole in lysis buffer). Finally, eluted protein was further purified by running a HiLoadSuperdex 200 (GEHealthcare 28989335) column with S200 buffer (25 mM Tris-HCl at pH 7.5, 500 mM NaCl, 5% glycerol).

Differential scanning fluorimetry assay

Purified WT-DIMT1 and 5mutA-DIMT1 proteins were diluted to 1 mg/mL in S200 buffer (25 mM Tris-HCl at pH 7.5, 500 mM NaCl, 5% glycerol). Nineteen microliters of each protein was transferred to one well in a 384-well plate, and 1 μL of fivefold SYPRO Orange (Thermo Fisher S6650) was added to each well. The plate was sealed and spun at 3600*g* for 2 min. The fluorescent signal at 570 nm was recorded using a RT-qPCR machine, with the temperature ramping from 20°C to 95°C. The data were analyzed using DSF World (Wu et al. 2020).

Competition assay

To perform the proliferation-based cellular competition assay, Cas9-expressing human cell lines of interest were transduced with sgRNA coexpressed with GFP as a marker for transduction. To deplete DIMT1, sgDIMT1#1 (GTAGTGCTGGAAGTTG GACC) and sgDIMT1#2 (ACAGTCATGTTGCCAGTTCC) were used, while sgRosa and sgPCNA were used as negative and positive controls, respectively. The number of GFP-positive cells was measured every second day starting from day 3 after infection using a Guava Easy 5HT instrument (Luminex 0500-4005). The percentage of GFP-positive cells on each day was normalized to the percentage of GFP-positive cells on day 3 after infection. The competition assays were performed in three biological replicates each in two technical replicates.

EMSA

A FAM-labeled RNA probe (5′-rUrUrCrCrGrUrArGrGrUrGrArArCrCrUrGrCrGrGrArA-3′) was dissolved in RNase-free water at 100 μM and diluted to 1 μM in EMSA binding buffer (25 mM Tris-HCl at pH 7.2, 150 mM NaCl, 40 U/mL RNasin). WT-DIMT1 and 5mutA-DIMT1 were diluted to a concentration series of 0.1, 0.5, 1, 2, 4, and 6 μM in EMSA binding buffer. One microliter of RNA probe and 1 μL of protein were mixed with 8 μL of binding buffer and incubated for 30 min on ice. The entire 10-μL RNA–protein mixture was then loaded onto a 4% TBE gel with 2.5 μL of loading buffer (1% bromophenol blue, 50% glycerol) and run at 120 V for 35 min at 4°C. The gel was imaged using an Amersham Typhoon 5 (Cytiva 29187191) fluorescent scan with a 473-nm laser. Quantification was carried out using Fiji ImageJ to quantify the intensity of the bottom free RNA band. The K_D (dissociation constant) was calculated in Prism with nonlinear curve fitting (allosteric sigmoidal) with the equation $y = V_{max} \times x^h/(K_{half}{}^h + x^h)$, where y is the bound fraction, x is the concentration of DIMT1 (in micromolar), V_{max} is set to 1, h is the hill slope, and K_{half} is the DIMT1 concentration resulting in 0.5 bound fraction.

RNA isolation

Total RNA was extracted from cell pellets using TRIzol reagent (Invitrogen 15596026) according to the manufacturer's instructions. To isolate 18*S* rRNA, 5 μg of total RNA was denatured in RNA loading dye (Thermo Fisher R0641) for 10 min at 72°C and run on a 1% TBE agarose gel. The 18S rRNA band was then excised from the gel and purified using a gel RNA recovery kit (Zymoclean R1011).

Quantitative analysis of the $m_2{}^{6,6}A$ level

Purified RNA was digested and dephosphorylated to single nucleosides using nucleoside digestion mix (NEB M0649S) for 2 h at 37°C. The nucleosides were quantified using retention time and nucleoside-to-base ion mass transitions of 268.0→136.0 (A), 284.0→152.0 (G), and 296.0→164.1 ($m_2{}^{6,6}A$). The percentage ratio of $m_2{}^{6,6}A$ to A was then used to compare the different modification levels between samples. LC-MS/MS data were analyzed using Skyline software.

In vitro methylation assays

The in vitro methylation assays were performed in a 30-µL reaction mixture containing the following components: 4 µg of biotinylated RNA probe 3′-rUrArGrGrUrGrArArCrCrUrG-5′ (0.945 nmol), 0.7875 nmol of protein, 1 mM SAM, 50 mM Tris-HCl (pH 7.5), 5 mM $MgCl_2$, and 1 mM DTT. The reaction mixture was incubated for 10 h at 16°C. After incubation, streptavidin beads (Thermo Scientific 10608D) were used to purify the RNA probe according to the manufacturer's instructions and eluted with 18.5 µL of RNase-free water for 5 min at 75°C.

Immunofluorescence microscopy

DIMT1$^{+/-}$ HEK293T cells expressing exogenous DIMT1 were grown in a six-well plate on top of a cover slide. Cells were rinsed once with 1× PBS followed by a 15-min rocking incubation with 1 mL of 4% formaldehyde in PBST (1× PBS, 0.05% Tween-20). Next, cells were incubated in 0.5% Triton in 1× PBST for 20 min followed by rinsing with PBST. Cells were then blocked in 1% BSA in PBST for 1 h followed by 1 h in primary anti-FLAG antibody (1:1000; MA1-142) and incubation in 1% BSA in PBST. Cells were then rinsed with 1% BSA in PBST followed by a 1-h incubation in antirat secondary antibody (1:300; A-11006). After secondary incubation, cells were rinsed with PBST followed by 1 min of incubation with 0.5 µg/mL DAPI and another PBST rinse. Twenty microliters of antifade reagent (P36970) was then applied to a microscope slide, and the coverslip was sealed on top. Microscope slides were then imaged on a Leica TCS SP8 confocal microscope.

Fluorescence recovery after photobleaching (FRAP)

All FRAP assays were performed using the bleaching module of the Zeiss LSM 880 confocal microscope. The 488-nm laser was used to bleach the mClover signal. Bleaching was focused on a circular region of interest (ROI) using 100% laser power, and time-lapse images were collected afterward. Additionally, a circular area of the same size outside the bleaching point was used as an unbleached control. The fluorescence intensity was directly measured in the Zen software (Zeiss). The values are reported as relative to prebleaching time points. GraphPad Prism was used to plot the data. The halftime for each replicate was calculated using a nonlinear one-phase association fit using the equation $Y = Y_0 + (\text{plateau} - Y_0) \times [1 - \exp(-K \times x)]$, in which plateau – Y_0 is the slow recovery fraction, K is the recovery rate, and the halftime is $ln(2)/K$. The mobile fraction is represented as the plateau.

To perform in vitro FRAP experiments, 30 µL of in vitro LLPS reaction was set up at room temperature with 25 mM Tris-HCl and NaCl concentrations of 50, 100, 200, 400, and 500 mM; DIMT1-mClover at 12.5 µM; and total RNA at 0, 16.7, 33.3, and 100 ng/µL. Reactions were incubated for 20 min at room temperature, transferred to a 384-well glass-bottom reader plate, and spun at 100*g* for 1 min. Images were taken using a Zeiss LSM 880 confocal microscope under a 20× lens.

The cellular FRAP was performed on HEK293T cells expressing DIMT1-mClover constructs cultured in glass-bottom dishes (MatTek P35GC). The media was changed with FluoroBrite DMEM (Thermo Scientific A1896701), and cells were incubated with one drop of NucBlue Live ReadyProbes reagent (Thermo Scientific R37605) for 1 min before imaging with a Zeiss LSM 880 confocal microscope under a 20× lens.

Protein quantitation and Western blotting

Protein concentrations were determined by Bradford assay (Bio-Rad 5000006). Fifty micrograms of protein samples was boiled for 5 min at 95°C in 1× Laemmli sample buffer , loaded onto SDS-PAGE gel, and run at 180 V for 1 h. Samples were transferred onto PVDF membranes using a semidry transfer apparatus at 20 V (sequences are listed in Supplemental Table S1) for 50 min. Membranes were then blocked with 3% milk in PBST followed by primary antibody incubation in 3% milk in PBST. Membranes were then rinsed with PBST followed by secondary incubation. The membranes were then washed with PBST and visualized using an ECL Western blotting detection kit (Thermo Fisher 34577).

AlphaFold structure analysis

The DIMT1-5mutA amino acid sequence was input into AlphaFold's ColabFold program. The resulting output PyMol file was compared with the solved crystal structure of WT-DIMT1 and the AlphaFold protein structure database model of WT-DIMT1. PyMol's superimpose command was then used to determine how closely folded the different structures were.

Ribosome profiling

MOLM-13C were transduced with sgDIMT or sgRosa coexpressed with GFP as a transduction marker in three biological replicates. The efficiency of lentivirus transduction was estimated by counting the number of GFP-positive cells using a Guava Easy 5HT instrument (Luminex 0500-4005). Depletion of DIMT1 was confirmed by Western blotting. On day 5 after infection, cells were treated with 100 µg/mL cycloheximide (CHX) for 7 min. The cells were harvested by spinning at 400*g* for 5 min and then washed once with ice-cold PBS supplemented with 100 µg/mL CHX. The collected cell pellets were resuspended in lysis buffer (10 mM Tris-HCl at pH 7.4, 150 mM KCl, 5 mM $MgCl_2$, 100 mg/mL CHX, 0.5% Triton X-100, protease inhibitor cocktail, RNase inhibitor, 100 µg/mL CHX) and kept for 15 min on ice, followed by centrifugation at 13,000 rpm for 15 min at 4°C. For the input library construction, 10 µL of 10% SDS was added to 100 µL of the cell lysis aliquot, and the Zymo Research RNA Clean and Concentrator-25 kit was used to purify total RNA. On the other hand, to digest mRNA not protected by ribosome, 120 U of RNase I (Ambion) of the cell lysate ($\text{absorbance}_{260\ \text{nm}} = 3$) was incubated for 30 min on ice. The reaction was stopped by addition of SUPERase:In (Ambion). To obtain ribosome-protected fragments (RPF), the digested lysate was loaded onto 10%–50% (w/v) sucrose gradient prepared in the lysis buffer without Triton X-100 by the Gradient Master (BioCamp). The gradients were centrifuged at 38,300 rpm for 2.75 h at 4°C in a SW-40Ti (Beckman) rotor using an Optima XE-100 ultracentrifuge (Beckman). Next, the gradient was fractionated into 1 mL by a Biocomp piston fractionator with a TRIAX flow cell for continuous UV detection at 256 nm and the monosome fractions were pooled, followed by RNA purification with the Zymo Research RNA Clean and Concentrator-25 kit. Obtained RNA was depleted of rRNA with the Ribo-minus kit (Invitrogen), separated in 15% TBE-urea gel, and stained with ethidium bromide. Gel slices containing nucleic acids 27–30 nt were excised and purified using the Zymo small RNA gel purification kit. To prepare the input samples, RNA >200 nt was extracted from the total RNA using RNA extraction kit (Zymo Research R1013). Purified RNA was then fragmented using an RNA fragmentation reagent kit (Invitrogen). Prior to library construction, both input sample RNA and RPF RNA were subjected to RNA end repair under PNK treatment (Thermo Fisher). Libraries were constructed according to the

NEBNext small RNA library preparation kit (NEB) protocol. The concentrations for all of the libraries were determined by the KAPA library quantification kit (KAPA Biosystems) according to the manufacturer's protocol and subjected to next-generation high-throughput sequencing using an Illumina NextSeq 550 with a single-end 75-bp read length.

Data analysis

The high-throughput sequencing reads were subjected to adaptor trimming using Trimmomatic (Bolger et al. 2014) with the following command: trimmomatc SE -phred33 ILLUMINACLIP: TruSeq3-SE.fa:2:30:10 MAXINFO:20:0.5 MINLEN:20. Reads mapping to rRNA, tRNA, and mtDNA were first cleaned using Bowtie2. The rRNA sequences were downloaded from the gene bank. The tRNA sequences were downloaded from the gtRNA database. The mtDNA sequences were directly obtained from the whole genome sequence. Next, the clean reads were mapped to genome GRCh38 using STAR (Dobin et al. 2013) with the following command: STAR –runThreadN 8 –alignSJDBoverhangMin 1 –alignSJoverhangMin 51 –outFilterMismatchNmax 2 –alignEndsType EndToEnd –readFilesCommand gunzip -c –outFileNamePrefix –quantMode GeneCounts –outSAMtype BAM SortedByCoordinate –limitBAMsortRAM 31532137230 –outSAMattributes All. Last, featureCounts (Liao et al. 2014) was used to count the read numbers for each gene. The differential translation efficiency and gene expression were calculated using DESeq2 (Love et al. 2014) according to the instructions from a previously reported procedure (Chothani et al. 2019).

Northern blots

Ten micrograms of total RNA was resolved on a denaturing 1.25% agarose gel containing 6.7% formaldehyde. The RNA was transferred overnight onto a Hybond N membrane by passive transfer in 20× saline–sodium citrate. After UV cross-link, RNA was probed for pre-rRNAs using P^{32}-labeled oligonucleotides targeting ITS1 (CCTCGCCCTCCGGGCTCCGTTAATGATC) or ITS2 (GGGGCGATTGATCGGCAAGCGACGCTC). Membranes were hybridized overnight at 65°C, washed, and dried prior to exposure and signal detection in a Typhoon FLA 9500 (GE Healthcare) phosphoimager. The pre-rRNAs were quantified and normalized to the mature 28*S* rRNA (EtBr or methylene blue staining) and then to the control samples (sgRosa).

Polysome profiling followed by qRT-PCR

MOLM-13C cells expressing WT-DIMT1, E85A-DIMT1, or 5mutA-DIMT1 on day 5 after infection with sgDIMT1 were treated with 100 μg/mL cycloheximide (CHX) for 7 min. The cells were harvested by spinning at 400*g* for 5 min and then washed with ice-cold PBS supplemented with 100 μg/mL CHX. The collected cell pellets were resuspended in lysis buffer (10 mM Tris-HCl at pH 7.4, 150 mM KCl, 5 mM $MgCl_2$, 100 mg/mL CHX, 0.5% Triton X-100, protease inhibitor cocktail, RNase inhibitor, 100 μg/mL CHX) and kept for 15 min on ice, followed by centrifugation at 13,000 rpm for 15 min at 4°C. The lysates were loaded on top of 10%–50% (w/v) sucrose gradient prepared in the lysis buffer without Triton X-100 by the Gradient Master (BioCamp). The gradients were centrifuged at 38,300 rpm for 2.75 h at 4°C in a SW-40Ti (Beckman) rotor using an Optima XE-100 ultracentrifuge (Beckman). Next, the gradients were fractionated into 1 mL by a Biocomp piston fractionator with a TRIAX flow cell for continuous UV detection at 256 nm. After fractionation, 200 μL of the light fraction (fraction 1) and 200 μL of the heavy fractions (pooled fractions 5–12) were subjected to RNA extraction. To have a normalization control, 0.2 ng of luciferase mRNA was spiked in prior to each RNA extraction. Extracted RNA from light and heavy fractions was subjected to qRT-PCR using a Luna RT-qPCR kit (NEB).

Data availability

The sequence data have been deposited in the NCBI GEO database under accession code GSE197276. All other data are available on request. All of the primers and probes used in this study are listed in Supplemental Table S3.

Competing interest statement

The authors declare no competing interests.

Acknowledgments

This work was supported by National Institutes of Health (NIH) grants R35 GM133721, R01 HL160726, and RSG-22-064-01-RMC American Cancer Research Scholar and a Damon Runyon Innovator Award to K.F.L.; NIH grant R35 GM118090 to R.M.; NIH grant R01 CA258904 to J. Shi; grant T32GM07133398 to K.S.; and Swiss National Science Foundation (SNSF) postdoctoral fellowship P2BEP3_200056 to Y.G. We thank Dr. Matthew Kayser for sharing the Leica SP8 confocal microscope, and Dr. Brain Capell for sharing the Nextseq550 sequencer.

Author contribution: J. Stoute, Y.G., H.S., and K.F.L. designed the experiments. Y.G. prepared the Ribo-seq samples. Y.G., K.B., and B.P. performed the competition-based proliferation assays with guidance from J. Shi H.S. processed the Ribo-seq data. J. Stoute, Y.G., and H.S. generated the constructs and the mammalian cell lines used in this study. J. Stoute, Y.G., and H.S. purified the recombinant DIMT1 (full-length proteins and the truncation variants) used in this study. J. Stoute performed the immunofluorescence imaging experiments and analyzed the data. J. Stoute, Y.G., and H.S. wrote the manuscript together with K.F.L. All authors participated in the discussion and editing of the manuscript.

References

Amin MA, Matsunaga S, Uchiyama S, Fukui K. 2008. Depletion of nucleophosmin leads to distortion of nucleolar and nuclear structures in HeLa cells. *Biochem J* **415:** 345–351. doi:10.1042/BJ20081411

Barros-Silva D, Klavert J, Jenster G, Jeronimo C, Lafontaine DLJ, Martens-Uzunova ES. 2021. The role of OncoSnoRNAs and ribosomal RNA 2′-O-methylation in cancer. *RNA Biol* **18:** 61–74. doi:10.1080/15476286.2021.1991167

Boehringer D, O'Farrell HC, Rife JP, Ban NN. 2012. Structural insights into methyltransferase KsgA function in 30S ribosomal subunit biogenesis. *J Biol Chem* **287:** 10453–10459. doi:10.1074/jbc.M111.318121

Bolger AM, Lohse M, Usadel B. 2014. Trimmomatic: a flexible trimmer for illumina sequence data. *Bioinformatics* **30:** 2114–2120. doi:10.1093/bioinformatics/btu170

Chaker-Margot M, Hunziker M, Barandun J, Dill BD, Klinge S. 2015. Stage-specific assembly events of the 6-MDa small-subunit processome initiate eukaryotic ribosome biogenesis. *Nat Struct Mol Biol* **22:** 920–923. doi:10.1038/nsmb.3111

Chaker-Margot M, Barandun J, Hunziker M, Klinge S. 2017. Architecture of the yeast small subunit processome. *Science* **355:** eaal1880. doi:10.1126/science.aal1880

Chothani S, Adami E, Ouyang JF, Viswanathan S, Hubner N, Cook SA, Schafer S, Rackham OJL. 2019. deltaTE: detection of translationally regulated genes by integrative analysis of Ribo-seq and RNA-seq data. *Curr Protoc Mol Biol* **129:** e108. doi:10.1002/cpmb.108

Desrosiers RC, Friderici KH, Rottman FM. 1974. Identification of methylated nucleosides in messenger RNA from Novikoff hepatoma cells. *Proc Natl Acad Sci* **71:** 3971–3975. doi:10.1073/pnas.71.10.3971

Desrosiers RC, Friderici KH, Rottman FM. 1975. Characterization of Novikoff hepatoma mRNA methylation and heterogeneity in the methylated 5′ terminus. *Biochemistry* **14:** 4367–4374. doi:10.1021/bi00691a004

Dobin A, Davis CA, Schlesinger F, Drenkow J, Zaleski C, Jha S, Batut P, Chaisson M, Gingeras TR. 2013. STAR: ultrafast universal RNA-seq aligner. *Bioinformatics* **29:** 15–21. doi:10.1093/bioinformatics/bts635

du Toit A. 2016. Expanding the mRNA epitranscriptome. *Nat Rev Mol Cell Biol* **17:** 201–201. doi:10.1038/nrm.2016.35

Feric M, Vaidya N, Harmon TS, Mitrea DM, Zhu L, Richardson TM, Kriwacki RW, Pappu RV, Brangwynne CP. 2016. Coexisting liquid phases underlie nucleolar subcompartments. *Cell* **165:** 1686–1697. doi:10.1016/j.cell.2016.04.047

Frye M, Blanco S. 2016. Post-transcriptional modifications in development and stem cells. *Development* **143:** 3871–3881. doi:10.1242/dev.136556

Gao K, Oerlemans R, Groves MR. 2020. Theory and applications of differential scanning fluorimetry in early-stage drug discovery. *Biophys Rev* **12:** 85–104. doi:10.1007/s12551-020-00619-2

Gilbert WV, Bell TA, Schaening C. 2016. Messenger RNA modifications: form, distribution, and function. *Science* **352:** 1408–1412. doi:10.1126/science.aad8711

Helser TL, Davies JE, Dahlberg JE. 1971. Change in methylation of 16S ribosomal RNA associated with mutation to kasugamycin resistance in *Escherichia coli*. *Nat New Biol* **233:** 12–14. doi:10.1038/newbio233012a0

Ikeda S, Kitadate A, Abe F, Saitoh H, Michishita Y, Hatano Y, Kawabata Y, Kitabayashi A, Teshima K, Kume M, et al. 2017. Hypoxia-inducible microRNA-210 regulates the DIMT1–IRF4 oncogenic axis in multiple myeloma. *Cancer Sci* **108:** 641–652. doi:10.1111/cas.13183

Ikeda S, Kitadate A, Abe F, Takahashi N, Tagawa H. 2018. Hypoxia-inducible KDM3A addiction in multiple myeloma. *Blood Adv* **2:** 323–334. doi:10.1182/bloodadvances.2017008847

Janin M, Coll-SanMartin L, Esteller M. 2020. Disruption of the RNA modifications that target the ribosome translation machinery in human cancer. *Mol Cancer* **19:** 70. doi:10.1186/s12943-020-01192-8

Janker L, Mayer RL, Bileck A, Kreutz D, Mader JC, Utpatel K, Heudobler D, Agis H, Gerner C, Slany A. 2019. Metabolic, anti-apoptotic and immune evasion strategies of primary human myeloma cells indicate adaptations to hypoxia. *Mol Cell Proteomics* **18:** 936–953. doi:10.1074/mcp.RA119.001390

Klinge S, Woolford JL. 2019. Ribosome assembly coming into focus. *Nat Rev Mol Cell Biol* **20:** 116–131. doi:10.1038/s41580-018-0078-y

Lafontaine D, Delcour J, Glasser AL, Desgres J, Vandenhaute J. 1994. The *DIM1* gene responsible for the conserved $m^6_2Am^6_2$-A dimethylation in the 3′-terminal loop of 18 S rRNA is essential in yeast. *J Mol Biol* **241:** 492–497. doi:10.1006/jmbi.1994.1525

Lafontaine DLJ, Riback JA, Bascetin R, Brangwynne CP. 2021. The nucleolus as a multiphase liquid condensate. *Nat Rev Mol Cell Biol* **22:** 165–182. doi:10.1038/s41580-020-0272-6

Lewis CJ, Pan T, Kalsotra A. 2017. RNA modifications and structures cooperate to guide RNA-protein interactions. *Nat Rev Mol Cell Biol* **18:** 202–210. doi:10.1038/nrm.2016.163

Liao Y, Smyth GK, Shi W. 2014. Featurecounts: an efficient general purpose program for assigning sequence reads to genomic features. *Bioinformatics* **30:** 923–930. doi:10.1093/bioinformatics/btt656

Love MI, Huber W, Anders S. 2014. Moderated estimation of fold change and dispersion for RNA-seq data with DESeq2. *Genome Biol* **15:** 550. doi:10.1186/s13059-014-0550-8

Mangat CS, Brown ED. 2008. Ribosome biogenesis; the KsgA protein throws a methyl-mediated switch in ribosome assembly. *Mol Microbiol* **70:** 1051–1053. doi:10.1111/j.1365-2958.2008.06484.x

Martin RM, Ter-Avetisyan G, Herce HD, Ludwig AK, Lättig-Tünnemann G, Cardoso MC. 2015. Principles of protein targeting to the nucleolus. *Nucleus* **6:** 314–325. doi:10.1080/19491034.2015.1079680

McMahon M, Contreras A, Ruggero D. 2015. Small RNAs with big implications: new insights into H/ACA snoRNA function and their role in human disease. *Wiley Interdiscip Rev RNA* **6:** 173–189. doi:10.1002/wrna.1266

Mills EW, Green R. 2017. Ribosomopathies: there's strength in numbers. *Science* **358:** eaan2755. doi:10.1126/science.aan2755

Nachmani D, Bothmer AH, Grisendi S, Mele A, Bothmer D, Lee JD, Monteleone E, Cheng K, Zhang Y, Bester AC, et al. 2019. Germline NPM1 mutations lead to altered rRNA 2′-O-methylation and cause dyskeratosis congenita. *Nat Genet* **51:** 1518–1529. doi:10.1038/s41588-019-0502-z

Narla A, Ebert BL. 2010. Ribosomopathies: human disorders of ribosome dysfunction. *Blood* **115:** 3196–3205. doi:10.1182/blood-2009-10-178129

O'Farrell HC, Scarsdale JN, Rife JP. 2004. Crystal structure of KsgA, a universally conserved rRNA adenine dimethyltransferase in *Escherichia coli*. *J Mol Biol* **339:** 337–353. doi:10.1016/j.jmb.2004.02.068

Poldermans B, Bakker H, Van Knippenberg PH. 1980. Studies on the function of two adjacent N^6, N^6-dimethyladenosines near the 3′ end of 16 S ribosomal RNA of *Escherichia coli*. IV. The effect of the methylgroups on ribosomal subunit interaction. *Nucleic Acids Res* **8:** 143–152. doi:10.1093/nar/8.1.143

Roundtree IA, Evans ME, Pan T, He C. 2017. Dynamic RNA modifications in gene expression regulation. *Cell* **169:** 1187–1200. doi:10.1016/j.cell.2017.05.045

Shen H, Stoute J, Liu KF. 2020. Structural and catalytic roles of the human 18S rRNA methyltransferases DIMT1 in ribosome assembly and translation. *J Biol Chem* **295:** 12058–12070. doi:10.1074/jbc.RA120.014236

Shen H, Gonskikh Y, Stoute J, Liu KF. 2021. Human DIMT1 generates $N_2^{6,6}$A-dimethylation-containing small RNAs. *J Biol Chem* **297:** 101146. doi:10.1016/j.jbc.2021.101146

Singh S, Vanden Broeck A, Miller L, Chaker-Margot M, Klinge S. 2021. Nucleolar maturation of the human small subunit processome. *Science* **373:** eabj5338. doi:10.1126/science.abj5338

Sloan KE, Warda AS, Sharma S, Entian KD, Lafontaine DLJ, Bohnsack MT. 2017. Tuning the ribosome: the influence of rRNA modification on eukaryotic ribosome biogenesis and function. *RNA Biol* **14:** 1138–1152. doi:10.1080/15476286.2016.1259781

Tokuhisa JG, Vijayan P, Feldmann KA, Browse JA. 1998. Chloroplast development at low temperatures requires a homolog of

DIM1, a yeast gene encoding the 18S rRNA dimethylase. *Plant Cell* **10:** 699–711. doi:10.1105/tpc.10.5.699

Tu C, Tropea JE, Austin BP, Court DL, Waugh DS, Ji XH. 2009. Structural basis for binding of RNA and cofactor by a KsgA methyltransferase. *Structure* **17:** 374–385. doi:10.1016/j.str.2009.01.010

Vlachos A. 2017. Acquired ribosomopathies in leukemia and solid tumors. *Hematology Am Soc Hematol Educ Program* **2017:** 716–719. doi:10.1182/asheducation-2017.1.716

Wieckowski Y, Schiefelbein J. 2012. Nuclear ribosome biogenesis mediated by the DIM1A rRNA dimethylase is required for organized root growth and epidermal patterning in *Arabidopsis*. *Plant Cell* **24:** 2839–2856. doi:10.1105/tpc.112.101022

Willyard C. 2017. An epigenetics gold rush: new controls for gene expression. *Nature* **542:** 406–408. doi:10.1038/542406a

Wu T, Yu J, Gale-Day Z, Woo A, Suresh A, Hornsby M, Gestwicki JE. 2020. Three essential resources to improve differential scanning fluorimetry (DSF) experiments. bioRxiv doi:10.1101/2020.03.22.002543

Zhao BXS, Roundtree IA, He C. 2017. Post-transcriptional gene regulation by mRNA modifications. *Nat Rev Mol Cell Biol* **18:** 31–42. doi:10.1038/nrm.2016.132

Zorbas C, Nicolas E, Wacheul L, Huvelle E, Heurgué-Hamard V, Lafontaine DL. 2015. The human 18S rRNA base methyltransferases DIMT1L and WBSCR22–TRMT112 but not rRNA modification are required for ribosome biogenesis. *Mol Biol Cell* **26:** 2080–2095. doi:10.1091/mbc.E15-02-0073